Upper Atmosphere Research Satellite (UARS) MLS observation of mountain waves over the Andes

Jonathan H. Jiang and Dong L. Wu
Jet Propulsion Laboratory, California Institute of Technology, Pasadena, California, USA

Stephen D. Eckermann
Middle Atmosphere Dynamics Section, Naval Research Laboratory, Washington, D. C., USA

Received 14 January 2002; revised 1 March 2002; accepted 5 March 2002; published XX Month 2002.

[1] Stratospheric air temperature (radiance) fluctuations over the Andes observed by the Upper Atmosphere Research Satellite (UARS) Microwave Limb Sounder (MLS) are presented. The MLS radiance variances show strong annual variability over the Andes mountains in South America, which is closely correlated to the background wind conditions associated with mountain wave generation and propagation. The variances are significantly larger in southern hemispheric winter when the winds in the troposphere and stratosphere over the Andes are both westerly and mountain wave critical levels (zero-wind lines) are absent. The annual variation of MLS radiance variance agrees well with data from radiosondes and output from the Naval Research Laboratory (NRL) Mountain Wave Forecast Model (MWFM) over the same region and period. The amplitude of the radiance variances seems to correlate well with the intensity of surface wind at upstream positions westward of the Andes, which is also related to the meridional temperature gradient in the region. Horizontal scale analysis suggests that mountain waves over the Andes might have two preferential horizontal wavelengths at $\sim$110 and $\sim$400 km. *INDEX TERMS:* 3337 Meteorology and Atmospheric Dynamics: Numerical modeling and data assimilation; 3334 Meteorology and Atmospheric Dynamics: Middle atmosphere dynamics (0341, 0342); 3360 Meteorology and Atmospheric Dynamics: Remote sensing

1. Introduction

[2] Mountain waves are internal gravity waves generated by vertically displaced air that flows over mountains. Air temperature fluctuations induced by such waves can be detected from space. *Eckermann and Preusse* [1999] and *Preusse et al.* [2002] showed significant stratospheric temperature oscillations observed over the Andes in infrared soundings from the Cryogenic Infrared Spectrometers and Telescopes for the Atmosphere (CRISTA) in November 1994. Recent analysis of Microwave Limb Sounder (MLS) data by *McLandress et al.* [2000] and GPS radio occultation data by *Tsuda et al.* [2000] and K. Hocke et al. (A study of stratospheric GW fluctuations and sporadic E at midlatitudes with focus on possible orographic effect of Andes, submitted to *Journal of Geophysical Research*, 2002) also showed enhanced temperature fluctuations in the stratosphere over the southern Andes. These observations provide strong indications that mountain waves induced by flow over the Andes may routinely reach the stratosphere and are observable with space borne limb-viewing techniques.

[3] The deposition of momentum flux from the breaking of such mountain waves makes significant contributions to the general circulation in the upper atmosphere [*McFarlane,* 1987]. Adequate consideration of mountain wave effects on the atmosphere by general circulation models improves the accuracy of numerical climate prediction and weather forecasts. In addition, in polar winter mountain waves can trigger formation of polar stratospheric clouds (PSCs) that leads to potential local decrease of the ozone mixing ratio through heterogeneous chemical reactions at low temperatures [*Carslaw et al.*, 1998a, 1998b]. Although mechanisms of mountain wave excitation and propagation have been examined by a number of individual modeling studies [e.g., *Sutherland and Linden,* 1998; *Satomura and Sato,* 1999; *Tan and Eckermann,* 2000], a thorough climatological understanding of mountain waves propagating into the stratosphere remains limited. Detailed observation and modeling are needed to quantify interactions between the background wind and topography.

[4] In this paper, we use the MLS limb-tracking 63 GHz radiance measurements [*Wu and Waters*, 1996b] to study mountain waves over the southern Andes. Section 2 outlines the radiance variance calculations; section 3 presents the MLS observations over the Andes. Section 4 investigates the role of background winds, critical levels, and surface climate conditions in modifying mountain wave generation and propagation into the stratosphere.

2. Radiance Variance Calculation

[5] The data used in this study are MLS saturated (i.e., optically thick) radiances from the O_2 line emission near

0148-0227/02/2002JD002091$09.00

63GHz. When saturated, MLS radiance variances provide a good measure of atmospheric temperature perturbations, although the magnitude of the radiance fluctuations is much weaker than the temperature amplitude due to MLS field-of-view averaging. For example, for gravity waves of 15 km vertical wavelength and horizontal sampling scale of ~100 km, the radiance variance is about 0.0036 times of the temperature variance [*Wu*, 2001].

[6] *Wu and Waters* [1996a, 1996b] applied a 6-point technique to compute radiance variances from MLS limb-scan data, in which the span of the six consecutive measurements is equivalent to a horizontal distance of about 90 km. Radiance variances at longer horizontal scales were truncated out very effective in this way. Also should be noted that these MLS variances are sensitive to waves of long (>10 km) vertical wavelengths [*Wu and Waters*, 1997]. *McLandress et al.* [2000] used a Fast Fourier Transform (FFT) method to compute variances from MLS limb-tracking data for horizontal scale of ≤480 km, but did not extend the study to mountain waves explicitly.

[7] MLS limb-tracking radiances were often acquired during 1995–1997, when the antenna pointing was fixed at a relatively constant tangent height below ~18 km where most radiances are saturated [*Wu and Waters*, 1996b]. Since the MLS viewing angle is 90° with respect to the satellite velocity, the horizontal separation between adjacent measurements is ~15 km, determined by the Upper Atmosphere Research Satellite (UARS) velocity and measurement time (2 seconds). About 40,000 radiance measurements are typically made on a limb-tracking day, and provide wave measurements over a wide range of horizontal scales.

[8] In this study, the limb-tracking radiance variances are computed differently using a set of "running-windows" to remove unwanted large-scale components. We first select a data sequence at a desired location and fill any data gaps using linear interpolation. Then, at a given height (channel) we compute the running window average $\{\bar{R}\}$ for each radiance sequence set $\{R\}$ as follows:

$$\bar{R}_i = \frac{1}{w}\sum_{j=0}^{w-1} R_{i+j-\mathrm{int}(w/2)}, \qquad i = \mathrm{int}\left(\frac{w}{2}\right), \ldots, N-w \qquad (1)$$

where N is the total number of individual measurements in $\{R\}$, w is width (number of data points) of the running window, or the horizontal window length, and must be an odd number. These running windows produce a set of filters that cut off radiance fluctuations of horizontal scales larger than $w \times 15$ kilometers. These filters are constructed by taking the difference between $\{R\}$ and $\{\bar{R}\}$, i.e.,

$$R'_i = R_i - \bar{R}_i, \qquad i = 0, \ldots, N-1. \qquad (2)$$

The radiance variance R'^2 of a region is the average of all individual R'^2_i in the region and a function of the truncation length w.

3. MLS Radiances Variances Over the Andes

[9] Radiance variances computed from different horizontal truncation windows contain mostly the wave power of horizontal scales less than the horizontal window length. For example, variances computed using 7-point truncation (representing the variances at horizontal scales ≤100 km) are similar to the results obtained by *Wu and Waters* [1996b]. The variance maps at this scale show a good correlation to stratospheric background winds, which is an effect of the refraction of gravity wave vertical wavelength into and out of the observational window by background wind (U and V) variations [*Alexander*, 1998]. Some regional patterns may indicate variability in gravity wave sources, such as those near deep-convection and surface topography [*McLandress et al.*, 2000].

[10] Figure 1a shows the map of MLS limb-tracking radiance variances at 48 km altitude for horizontal window length of 105 km (w = 7) for the period May–September 1995. The region highlighted by the white dashed curve (55°W–85°W, 30°S–50°S) is the "Andes region" that we focus on in this study. The maximum variance over the Drake Passage between the southern tip of South America and Antarctica is not considered here and will be addressed in a separate study: our preliminary analysis has shown that the seasonal behavior of this wave activity is closely related to that over the Andes region. Figures 1b and 1c are meridional and zonal distributions of the mean variances for the Andes region, respectively, where variance growth with altitude is evident up to ~60 km.

[11] The monthly mean variances averaged between 33–53 km over the Andes region are shown in the top panel of Figure 2. For comparison, the bottom panel of Figure 2 shows the monthly temperature variances averaged between 100 and 10 hPa (altitude ~16–32 km) from six radiosonde stations located inside the Andes region. Both the MLS and the radiosonde data show active-periods during May–September of both 1995 and 1996 with enhanced stratospheric temperature fluctuations possibly related to mountain wave activity over the Andes. It is also interesting to note that the intensity of temperature and radiance fluctuations during the two active periods is quite different. The one in 1995 is significantly more intense than that in 1996.

[12] Figure 3 shows the horizontal-scale dependence of MLS radiance variances over the Andes region, averaged during the active-periods in 1995 (left) and 1996 (right). The top panels illustrate the variances as a function of horizontal window length (in km), while the bottom panels show the derivatives of the variances. The derivatives are the rate of change of variances with respect to the horizontal window lengths. In general, the variance increases with the horizontal window length since more power is usually associated with waves of longer horizontal wavelengths. However, the variance derivatives can depend on the horizontal scale of the waves too. As illustrated in the bottom panels in Figure 3, the derivatives vary substantially at window lengths between 0 and 1000 km and show two clear peaks at horizontal scales <100 and ~350 km.

4. Discussion

4.1. The Role of Background Winds

[13] The time series of MLS radiance variances over the Andes (Figure 2) can be mostly explained by differences in the background winds. Figure 4 shows the United Kingdom Meteorological Office (UKMO) assimilated mean zonal

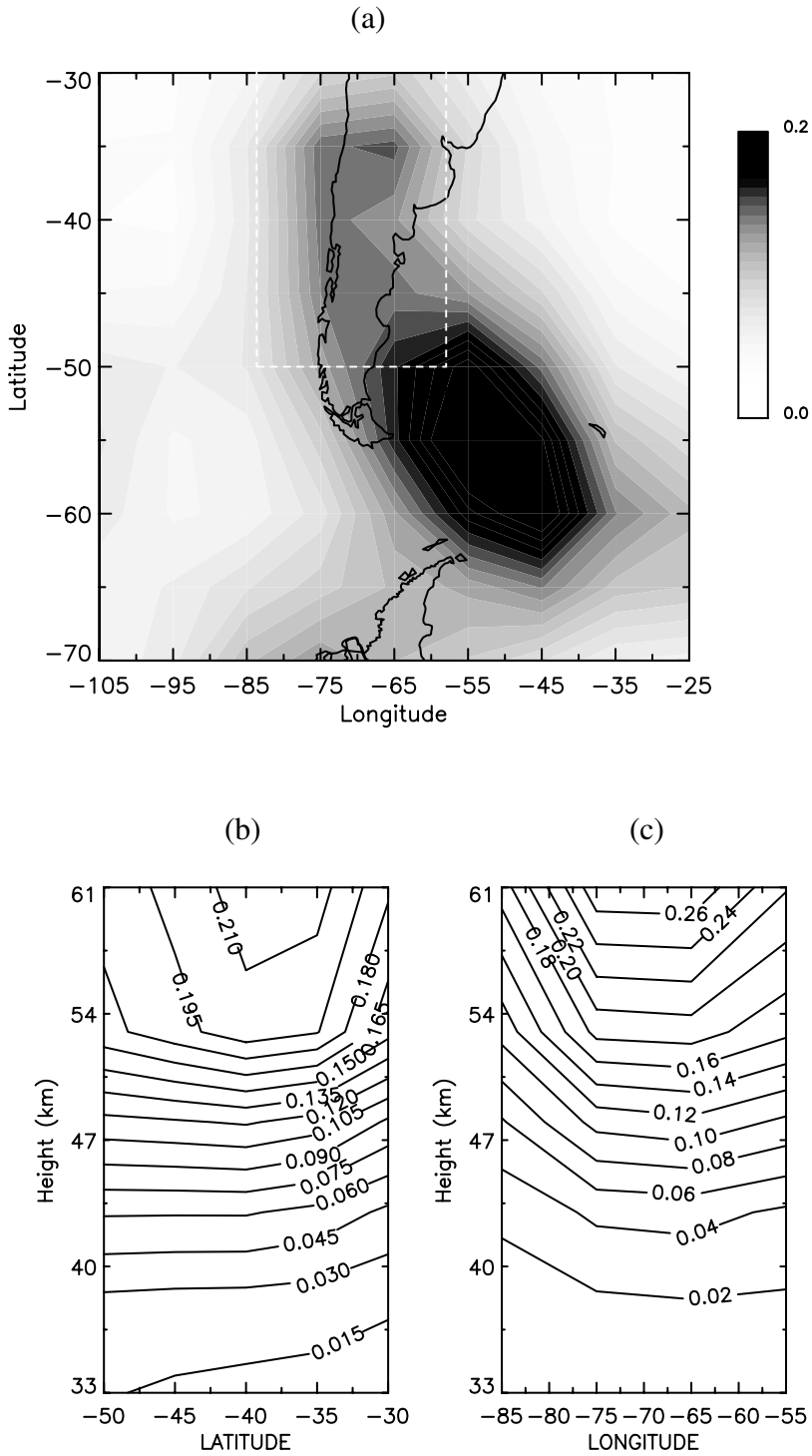

Figure 1. (a) May–September 1995 averaged MLS limb-tracking radiance variances (in units of K^2) at 48 km altitude, computed using a 105 km horizontal window length. The region enclosed indicates the focus area of interest in this investigation. (b) and (c) are meridional and zonal distributions of the mean variances for the Andes region, respectively.

wind (U) fields above the Andes region during the active- and quiet-periods. During the active-periods, the winds in the troposphere and stratosphere are both dominated by the westerlies and no mountain wave critical level (zero-wind-line) appears in this region. During the quiet-periods, the critical level is present at ~46 hPa (~22 km), which prevents mountain waves from propagating into the stratosphere. This is consistent with the annual cycle in Figure 2 and suggests that these fluctuations are dominated by mountain waves.

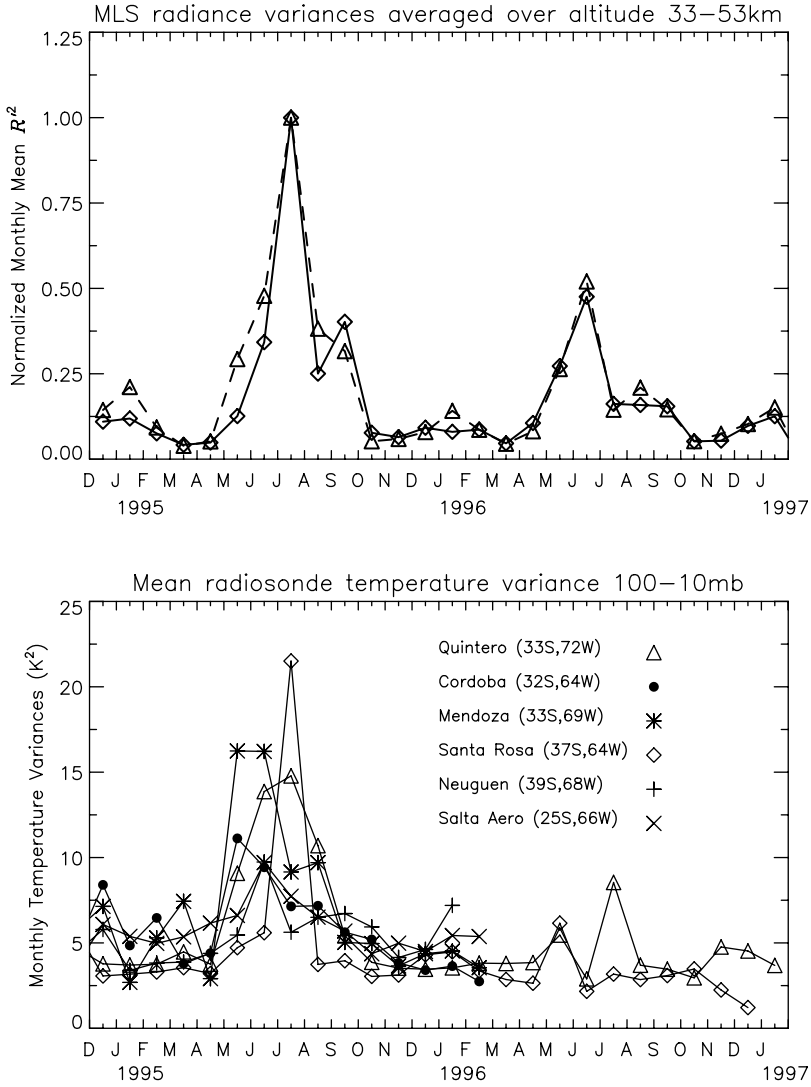

Figure 2. Top: monthly mean MLS radiance variances (normalized to unity) over the Andes. The triangles and squares show the variances computed by 105 km (solid-line) and 375 km (dashed-line) horizontal window lengths, respectively. Bottom: monthly air temperature variances averaged between 100 and 10 hPa, taken from measurements from six radiosonde stations located in/near the Andes region. The radiosonde temperature variances are calculated using all the measurements between 100 and 10 hPa with the mean and a linear trend removed.

[14] Interactions between propagating gravity waves and the background winds are the key mechanism for interpreting MLS radiance variances [*Alexander*, 1998; *Jiang and Wu*, 2001]. To the first order, one may relate the vertical wavelength to the horizontal wind speed in a simple form [e.g., *Eckermann*, 1995]:

$$\lambda_z = 2\pi(c - U\cos\theta)/N_{bf} \tag{3}$$

where c is the wave horizontal phase speed with respect to the ground, U is the horizontal background wind speed, θ is the angle between the wind and the wave propagation direction and N_{bf} is the buoyancy frequency. Usually, mountain waves can be assumed to be roughly stationary with respect to the ground (i.e., $c \sim 0$) and can only propagate when their horizontal phase speeds are nonzero with respect to the background flow (i.e., $c - U\cos\theta \neq 0$). At a mountain wave critical level ($c = 0$, $U = 0$), the vertical wavelength vanishes and waves are either absorbed and/or break down. Such a mechanism is supported by both the MLS variance observations and UKMO wind data during summer.

4.2. MWFM Simulation

[15] To further study the effect of local winds and temperatures on mountain wave evolution over the Andes, we used the Naval Research Laboratory (NRL) Mountain Wave Forecast Model (MWFM). *Bacmeister* [1993] and *Bacmeister et al.* [1994] describe the version 1 hydrostatic model: only salient details and extensions to version 2 are described here.

[16] MWFM is a parameterization that operates diagnostically on gridded atmospheric winds and temperatures. A

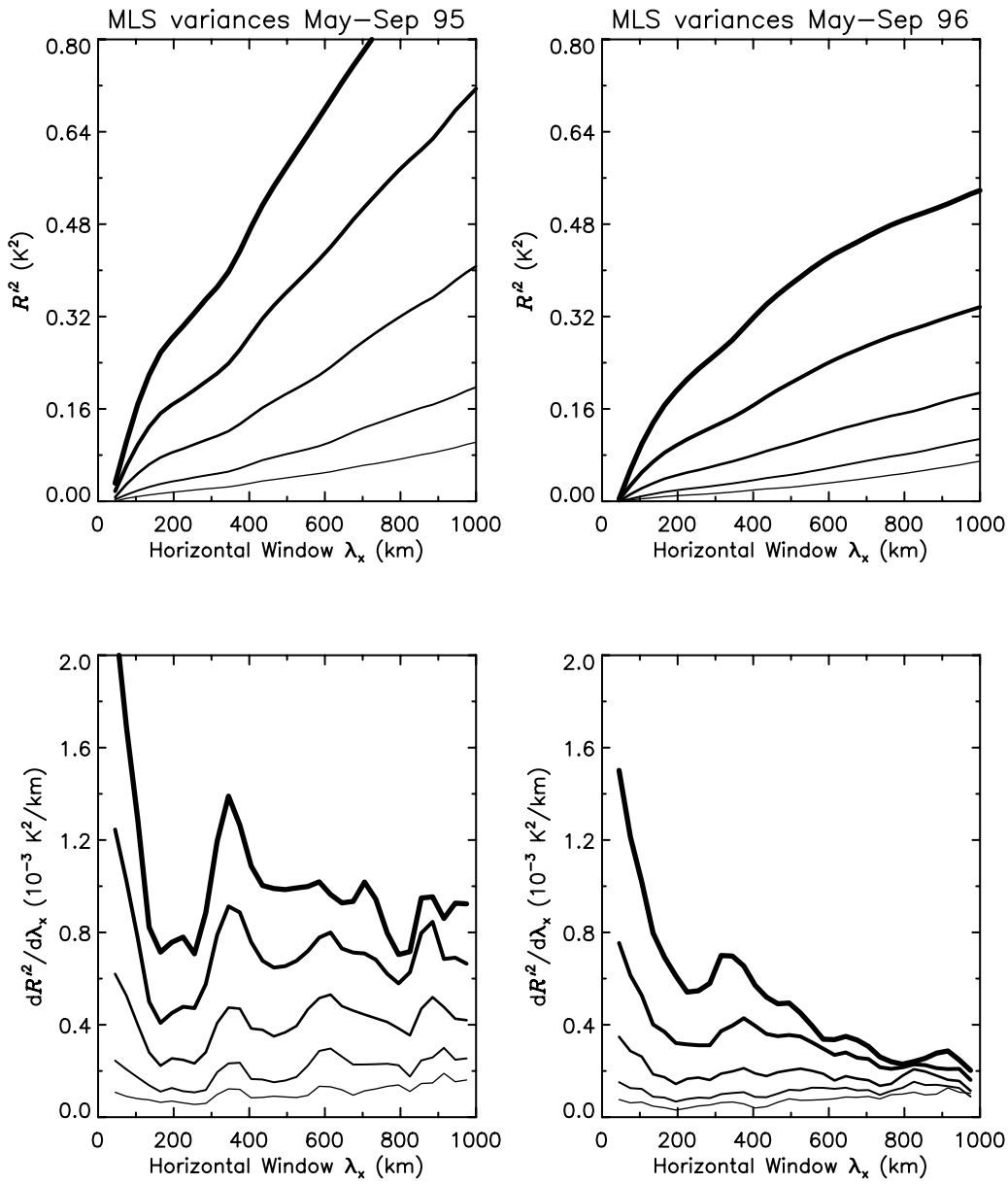

Figure 3. Horizontal-scale dependence of MLS radiance variances over the Andes region, averaged for the active-periods (May–September) of 1995 (left) and 1996 (right). The top panels illustrate the variances as a function of horizontal truncation length (in km), while the bottom panels show the derivative of the variances (or variances changing rate) with respect to the truncation length. The thickness of curves from light to dark indicates the data for five different altitudes of 38, 43, 48, 53, and 61 km.

key feature is the decomposition of global topography into a list of quasi-two-dimensional ridges, each with a characteristic width, length, height, horizontal orientation and quality (degree of two-dimensionality) that define the types of mountain waves forced by directional flow over the feature. Surface winds blowing over these ridges are used to calculate the spectrum of mountain waves at the surface. Vertical profiles of winds and temperatures determine subsequent propagation and amplitude evolution of these waves with height.

[17] Here we use the version 2.1 model (MWFM 2.1) that incorporates a number of improvements over version 1. The major change is that ray equations governed by a non-hydrostatic dispersion relation with rotation and density scale height [*Marks and Eckermann*, 1995] replace earlier hydrostatic irrotational wave equations. Only vertical atmospheric variations are retained in the ray equations: neglect of horizontal gradients and temporal atmospheric variations means, respectively, that horizontal wavenumbers k remain constant and ground-based phase speeds remain stationary ($c = 0$). This ray approach models mountain waves more accurately since it includes many more relevant physical processes: for example, it can reproduce full solutions to three-dimensional mountain wave problems, such as "ship wave" patterns in turning flow [*Broutman et al.*, 2001, 2002].

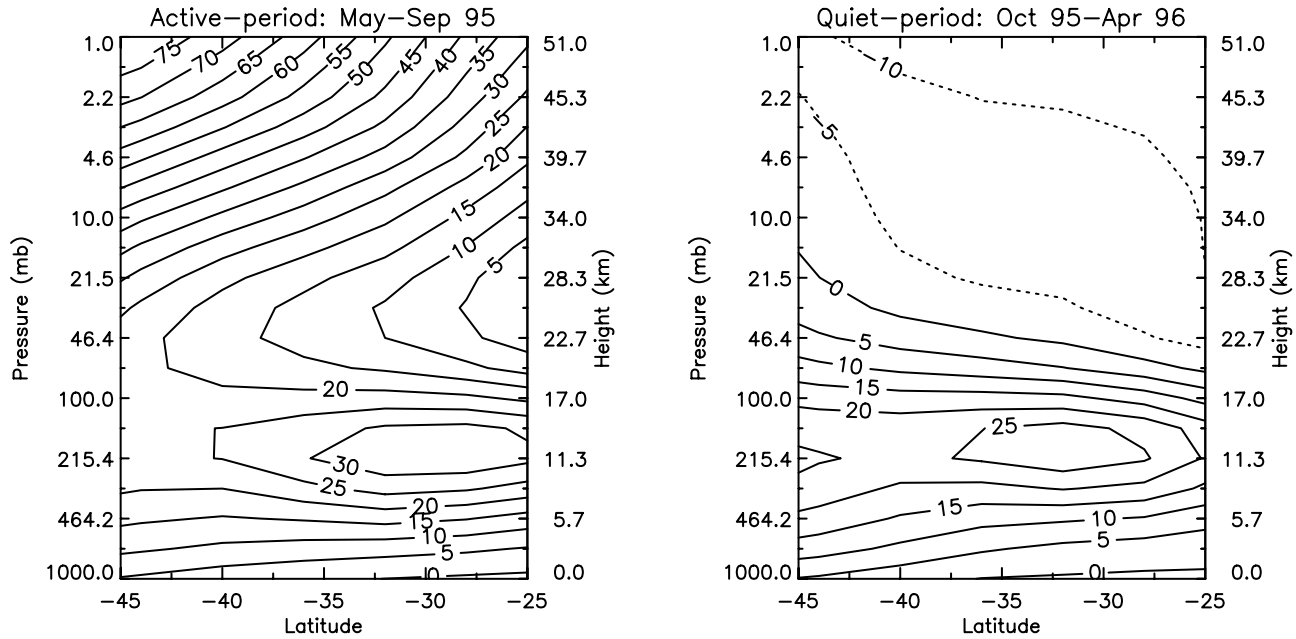

Figure 4. UKMO assimilated mean zonal wind fields averaged during limb-tracking days of the active-period (left) and quiet-period (right). Contour labels are in ms^{-1}.

[18] A spectrum of rays is launched from each ridge feature. In this study we launch 12 rays per ridge: 2 different horizontal wavenumbers k, each launched at 6 equispaced azimuths φ, centered about the intrinsic horizontal orientation of the ridge's short axis, to span the full azimuth range of 0–180°. In this study horizontal wavenumbers were set as k = 1.5 J/W where W is the width of the short axis of the ridge and J = 1, 2. Wave amplitudes were set according to the height of the ridge feature and were scaled with azimuth φ based on the ridge quality. In this way, highly two-dimensional ridges produced rays with significant amplitude orthogonal to the long ridge axis only, yielding a plane wave, whereas more three-dimensional ridges produced significant amplitudes at various azimuths and thus radiated

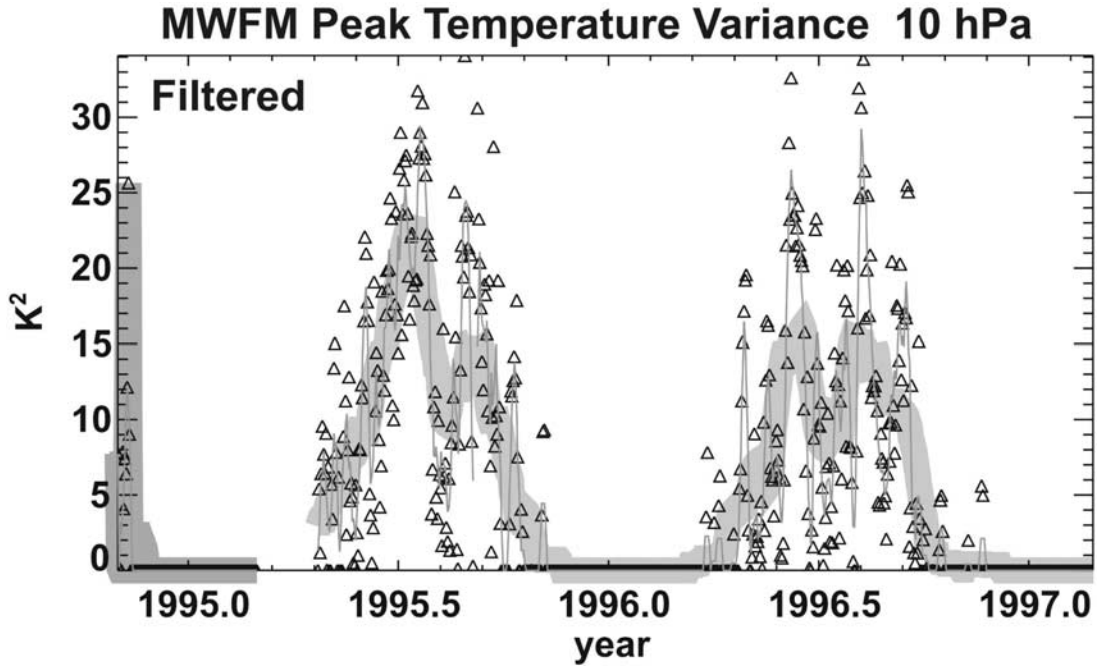

Figure 5. Gridbox averaged variance of peak mountain wave temperature amplitudes at 10 hPa (~32 km) over the Andes region (30°–50°S, 80°–50°W) due to MWFM-simulated mountain waves with vertical wavelengths >10 km and horizontal wavelengths >30 km. Triangles show daily values, thin solid line shows a 4-day running average, thick solid gray line shows a 30-day (monthly) running average.

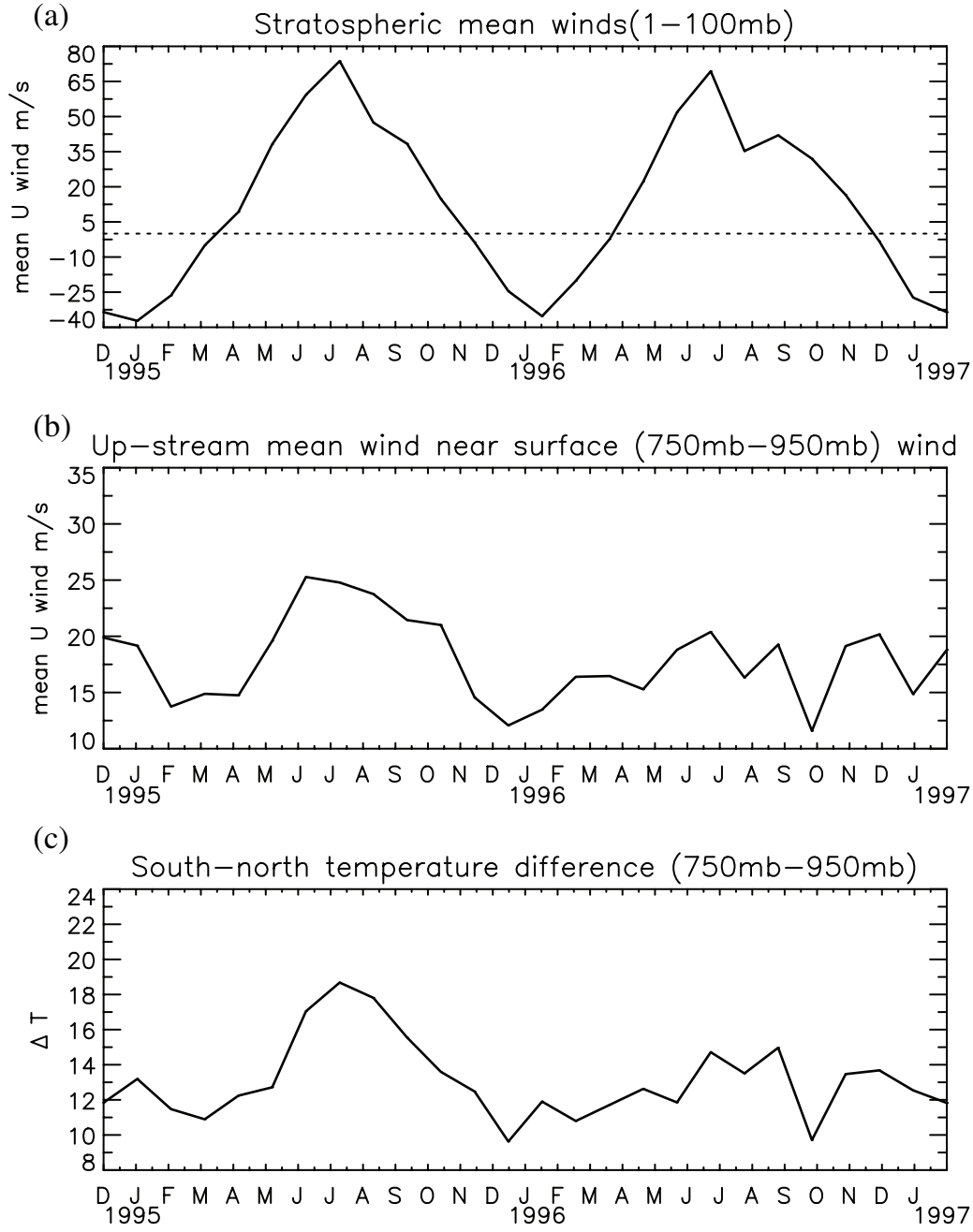

Figure 6. (a): UKMO assimilated monthly mean U winds averaged between 1 and 100 hPa over the Andes region; (b): UKMO near surface (750–950 hPa) monthly mean U winds averaged at up-stream location (85°W–95°W) of the Andes region; (c): near-surface monthly Andes region meridional mean temperature difference [T(25°S) − T(45°S)]. All data are averaged monthly over limb-tracking days.

more of a ship wave. As each ray propagates away from its parent ridge, along-ray amplitudes are governed by conservation of vertical flux of wave action density, subject to wave breaking thresholds based on dynamical and convective instability thresholds [see *Marks and Eckermann*, 1995]. For some examples of the use and output of the MWFM version 2 model, see *Eckermann and Preusse* [1999] and *Hertzog et al.* [2002].

[19] We ran MWFM 2.0 in "hindcast" mode over the Andes region at 12Z every day, starting on 1 November 1994 and finishing on 28 February 1997. We chose regional atmospheric winds and temperatures provided by NASA's Data Assimilation Office (DAO), due to the stronger stratospheric emphasis of these assimilations compared to other meteorological analyses. These DAO data are issued at 2.5° × 2° longitude-latitude resolution on 18 standard pressure levels between 1000 and 0.4 hPa. There were no data from 3 March to 23 April 1995, marking a changeover period from the "ASHOE/MAESA" to the "STRAT" series of assimilation runs (for further details, see *Coy and Swinbank* [1997]). The daily MWFM ray predictions of peak wave amplitudes squared at various pressure levels

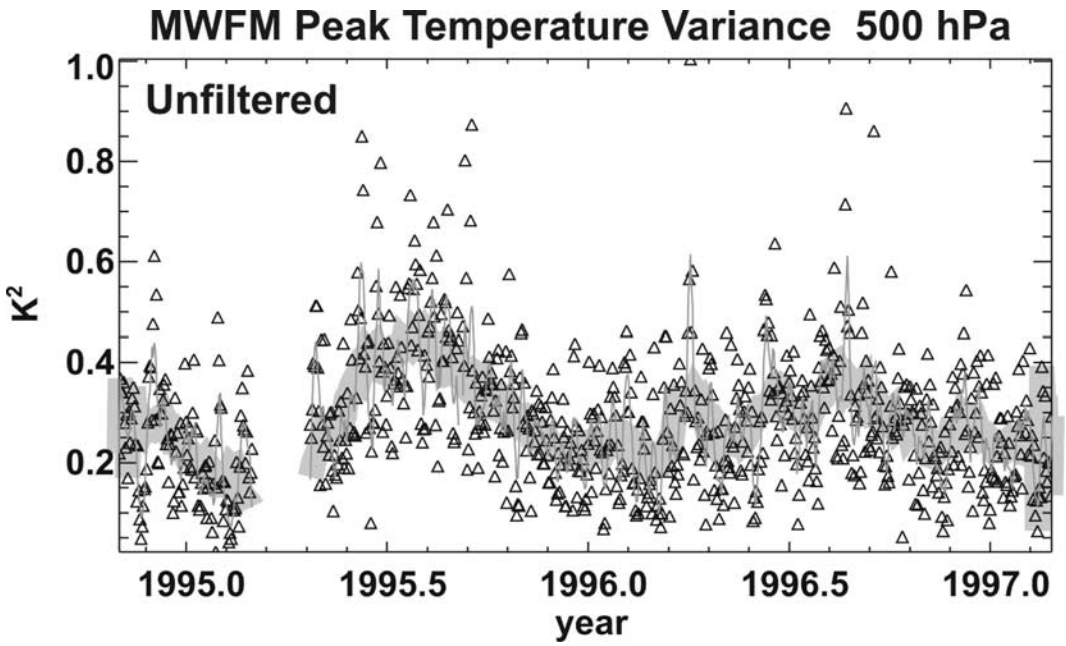

Figure 7. As for Figure 5, but showing MWFM results at 500 hPa (~4–5 km) for all mountain waves (no wavelength filtering) in the range 26°–36°S, 80°–50°W.

were averaged within 2.5° × 2° grid boxes and stored. A similar averaging procedure was used for the MWFM 2.0 runs in the northern hemisphere study of *Pierce et al.* [2002]. A range of simulations was conducted to assess sensitivity to various parameter choices as well as filtering of horizontal and/or vertical wavelengths to mimic MLS weighting functions.

[20] Figure 5 plots variations in gridbox-averaged rms peak MWFM temperature amplitudes due to mountain waves over the Andes region at 10 hPa (~32 km). These results filtered out all gravity waves with vertical wavelengths shorter than 10 km and horizontal wavelengths shorter than 30 km, roughly approximating the sensitivity of MLS to gravity waves [*Wu and Waters*, 1997; *Alexander*, 1998]. Thick curves are thirty-day running averages that mimic the monthly averages in Figure 2. MWFM results reproduce the strong annual cycle observed in Figure 2. They also reproduce the larger 1995 peak compared to 1996, as well as their relative magnitudes. Figure 5 also seems to reproduce the notch and secondary maximum in the 1995 MLS winter peak. A similar feature is generated in 1996 that is less evident in the MLS data, but for which there is some evidence in the radiosonde data in Figure 2. Little "tuning" of these MWFM simulations was performed and the results do not vary to any great extent with changes to the input source parameters, filter thresholds or averaging methods. The good agreement between model and observations here provides robust support for a mountain wave interpretation of the >2 years of MLS and radiosonde temperature variance over the Andes region in Figure 2.

[21] Another interesting feature of Figure 5 is that there are almost no MWFM-simulated mountain waves at 10 hPa over the Andes region during November–April. A prominent exception occurs in early November of 1994. Interestingly, this corresponds to the first CRISTA mission period when long stratospheric mountain waves were initially observed from orbit over the Andes [*Eckermann and Preusse*, 1999; *Preusse et al.*, 2002]. This event appears to have been facilitated by northward displacement of a well-defined late-spring vortex, so that the vortex edge lay over South America at this time [*Eckermann and Preusse*, 1999]. Figures 2 and 5 indicate that CRISTA in fact measured an uncommon late-spring stratospheric mountain wave burst, and thus, in retrospect, CRISTA's discovery of these waves at this time was somewhat fortuitous, since typically mountain waves are weak or absent at this time.

4.3. Upstream Wind Velocity and Meridional Temperature Gradient

[22] Although the stratospheric winds are crucial for mountain waves to reach the stratosphere, near surface (750–950 hPa) winds are another determining factor in the strength of mountain wave forcing over the Andes region. The different magnitudes of wave activity observed during the active periods of 1995 and 1996 can be due to either damping/filtering in wave propagation or different wave strengths during generation. According to UKMO assimilations, the monthly averaged propagation conditions in the stratosphere (i.e., zonal winds above ~100 hPa) are not much different between the active-periods in 1995 and in 1996 (Figure 6a), which implies that the damping and local stratospheric filtering are not sufficiently different to explain the variations in the variances. It is the variation of the near surface winds that seems somewhat more consistent with the observed variance modulation. As shown in Figure 6b, the near surface zonal winds (U winds) are stronger and less variable during the 1995 active-period, whereas during the 1996 active-period, the surface winds are weaker and more variable. We also find a sharper and stronger meridional V wind field just west of the Andes during the 1995 active-period, which may result from the

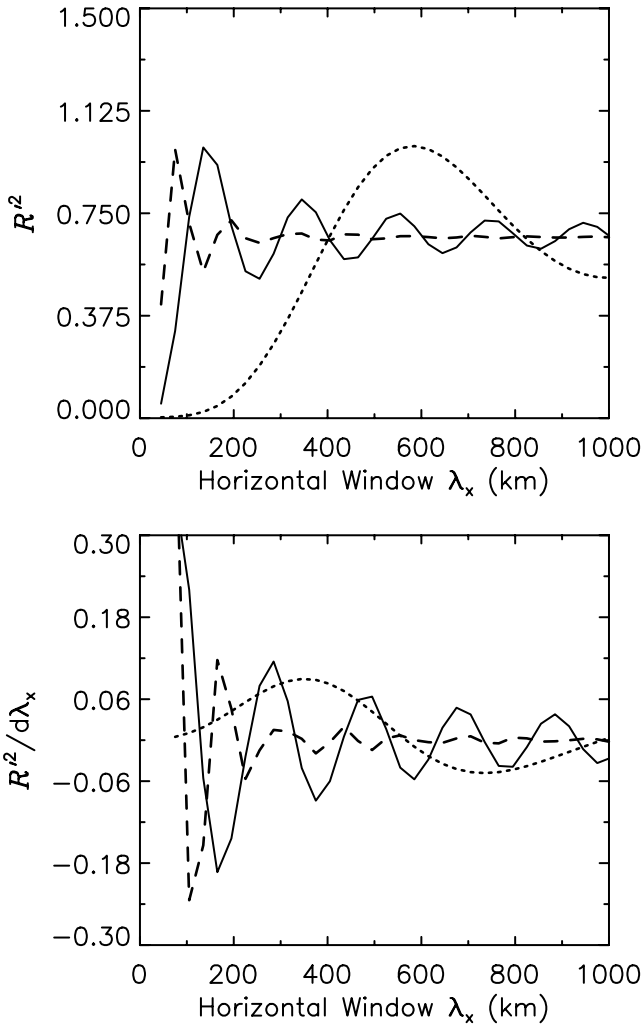

Figure 8. Simulations of three "red-noise" experiments produced by sine-waves of horizontal wavelengths λ = 50 km (dashed-line), 100 km (solid-line) and 400 km (dotted-line). The top-left panel shows the variances produced by the three "red-noise" experiments as a function of horizontal window length (in km), while the bottom-panel shows the derivatives of the "red-noises" variances with respect to the truncation length.

wind flow that is redirected meridionally by the Andes topography [see *Seluchi et al.*, 1998].

[23] Based on the thermal wind equation [*Holton*, 1979], the strength of the tropospheric quasi-zonal flow (primarily the U wind) is proportional to the meridional (equator-to-pole) temperature gradient. We found the near surface temperature gradient in 1995 near the Andes was generally larger than that in 1996 (Figure 5c). It is not clear what caused the larger meridional temperature gradient: one likely factor is the sea surface temperature anomaly in the eastern tropical Pacific, which can modulate the temperatures in the lower part of the atmosphere [*Alexander*, 1992; *Trenberth and Hoar*, 1996].

[24] To see if something similar emerges in the MWFM results, Figure 7 plots the unfiltered MWFM results (all ray data) at the lowest stored level of 500 hPa in the latitude band from 26°–36°S. We see a tendency for both an annual cycle peaked in winter as well as a stronger winter peak in 1995 relative to 1996. These findings are consistent with the low-level flow ideas expressed in Figures 6b and 6c. The features seen in Figure 7 disappear at more poleward latitudes, and averages of 500 hPa MWFM results over the 30°–50°S show little systematic seasonal or interannual variability. Thus this result seems to be restricted to the equatorward half of our region of interest.

4.4. Horizontal Scales of Mountain Waves

[25] What can we infer from the scale-dependent derivative of the MLS variances shown in Figure 3? To pursue this investigation, we first study characteristics of the running window filters using artificial wave oscillations. We generated sinusoidal radiance fluctuations at the same location as sampled by MLS and applied the same method to extract the variances for different horizontal window lengths. As shown in Figure 8, three wavelengths (50, 100, and 400 km) are used to examine the filter responses. The oscillations in Figure 8 are due to the ripple effects of the boxcar filter. Note that the second derivative peaks of the λ = 50 km and λ = 100 km waves are found at horizontal window lengths of ~150 and ~300 km, respectively, which is about three times the actual wavelengths. The λ = 400 km wave produces a broad derivative peak in the 300–500 km range of horizontal window lengths.

[26] These simulations on artificial data suggest that the "wave-filter" used in MLS variance analysis of section 2 is sensitive to horizontal wavelength. The scale-dependent derivatives in Figure 3 are statistically significant and may indicate that mountain waves over the Andes region have some dominant horizontal wavelengths. Re-examining Figure 3, we find that the first (<100 km) and second (~350 km) derivatives peaks (see bottom panels of Figure 3) may together be related to a preferential scale near 110 km since other scales (e.g., 50 km) would create a second ripple visible to MLS (e.g., 150 km). The broad but weak enhancement between 300 and 800 km may indicate another scale near 400 km associated with mountain waves over the Andes. These scales are in line with earlier inferences from CRISTA observations during November 1994 [*Eckermann and Preusse*, 1999], suggesting that the mountain waves over the Andes had a horizontal wavelength of either ~400 km or ~130 km. Subsequent modeling studies have provided some preliminary support for these observations [*Tan and Eckermann*, 2000; *Preusse et al.*, 2002].

5. Conclusion

[27] Significant enhancements of MLS radiance variances in the middle atmosphere (~33–53 km) are observed over the southern Andes during May–September in 1995 and 1996, when both the tropospheric and stratospheric winds are dominated by the westerlies without any zero-wind-line. Similar features are seen in stratospheric radiosonde temperatures. Application of a mountain wave model at this location for 1995–1996 strongly supports the interpretation of these features as mountain waves. During the active-period of 1995, the equator-to-pole near surface temperature gradient, the intensity of surface wind upstream of the Andes, and MLS radiance variances over the Andes

region are all considerably larger than those during the same period in 1996. This suggests that a climate anomaly event such as El Niño may play an important role in modulating the mountain wave generation and the wave intensity reaching the stratosphere, an idea that the mountain wave model lends some support to. Horizontal scale analyses of MLS radiance variances suggest that mountain waves over the Andes may have two preferred horizontal wavelengths near 110 and 400 km.

[28] **Acknowledgments.** The authors would like to thank the anonymous reviewers for very helpful comments and suggestions. JHJ and DLW performed the research at the Jet Propulsion Laboratory, California Institute of Technology, supported by the National Aeronautics and Space Administration (NASA). SDE acknowledges support from the Office of Naval Research and the NASA ACMAP program.

References

Alexander, M. A., Midlatitude atmosphere-ocean interaction during El Niño, *J. Clim.*, *5*, 944–972, 1992.

Alexander, M. J., Interpretations of observed climatological patterns in stratospheric gravity wave variance, *J. Geophys. Res.*, *103*, 8627–8640, 1998.

Bacmeister, J. T., Mountain-wave drag in the stratosphere and mesosphere inferred from observed winds and a simple mountain-wave parameterization scheme, *J. Atmos. Sci.*, *50*, 377–399, 1993.

Bacmeister, J. T., P. A. Newman, B. L. Gary, and K. R. Chan, An algorithm for forecasting mountain wave related turbulence in the stratosphere, *Weather Forecast.*, *9*, 241–253, 1994.

Broutman, D., J. W. Rottman, and S. D. Eckermann, A hybrid method for analyzing wave propagation from a localized source, with application to mountain waves, *Q. J. R. Meteorol. Soc.*, *127*, 129–146, 2001.

Broutman, D., J. W. Rottman, and S. D. Eckermann, Maslov's method for stationary ydrostatic mountain waves, *Q. J. R. Meteorol. Soc.*, in press, 2002.

Carslaw, K. S., et al., Particle microphysics and chemistry in remotely observed mountain polar stratospheric clouds, *J. Geophys. Res.*, *103*, 5785–5796, 1998a.

Carslaw, K. S., et al., Increased stratospheric ozone depletion due to mountain-induced atmospheric waves, *Nature*, *391*, 675–678, 1998b.

Coy, L., and R. Swinbank, Characteristics of stratospheric winds and temperatures produced by data assimilation, *J. Geophys. Res.*, *102*, 25,763–25,781, 1997.

Eckermann, S. D., Effect of background winds on vertical wavenumber spectra of atmospheric gravity waves, *J. Geophys. Res.*, *100*, 14,097–14,112, 1995.

Eckermann, S. D., and P. Preusse, Global measurements of stratospheric mountain waves from space, *Science*, *286*, 1534–1537, 1999.

Hertzog, A., F. Vial, A. Dörnbrack, S. D. Eckermann, B. M. Knudsen, and J.-P. Pommereau, In situ observations of gravity waves and comparisons with numerical simulations during the SOLVE/THESEO 2000 campaign, *J. Geophys. Res.*, *107*, 10.1029/2001JD001025, in press, 2002.

Holton, J. R., *An Introduction to Dynamic Meteorology*, 2nd ed., pp. 44–47, Academic, San Diego, Calif., 1979.

Jiang, J. H., and D. L. Wu, UARS MLS observation of gravity waves associated with the Arctic winter stratospheric vortex, *Geophys. Res. Lett.*, *28*, 527–530, 2001.

Marks, C. J., and S. D. Eckermann, A three-dimensional nonhydrostatic ray-tracing model for gravity waves: Formulation and preliminary results for the middle atmosphere, *J. Atmos. Sci.*, *52*, 1959–1984, 1995.

McFarlane, N. A., The effect of orographically excited gravity wave drag on the general circulation of the lower stratosphere and troposphere, *J. Atmos. Sci.*, *44*, 1775–1800, 1987.

McLandress, C., M. J. Alexander, and D. L. Wu, Microwave limb sounder observations of gravity waves in the stratosphere: A climatology and interpretation, *J. Geophys. Res.*, *105*, 11,947–11,967, 2000.

Pierce, R. B., et al., Large-scale chemical evolution of the Arctic vortex during the 1999–2000 winter: HALOE/POAM 3 Lagrangian photochemical modeling for the SAGE III Ozone Loss and Validation (SOLVE) Campaign, *J. Geophys. Res.*, *107*, 10.1029/2001JD001063, in press, 2002.

Preusse, P., A. Drnbrack, S. D. Eckermann, M. Piese, B. Schaeler, J. T. Bacmeister, D. Broutman, and K. U. Grossmann, Space-based measurements of stratospheric mountain waves by CRISTA, 1, Sensitivity, analysis method and a case study, *J. Geophys. Res.*, *107*, 10.1029/2001JD000699, in press, 2002.

Satomura, T., and K. Sato, Secondary generation of gravity waves associated with the breaking of mountain waves, *J. Atmos. Sci.*, *56*, 3847–3858, 1999.

Seluchi, M., Y. V. Serafini, and H. Le Treut, The impact of the Andes on transient atmospheric systems: A comparison between observations and GCM results, *Mon. Weather Rev.*, *126*, 895–912, 1998.

Sutherland, B. R., and P. F. Linden, Internal wave excitation from stratified flow over a thin barrier, *J. Fluid Mech.*, *377*, 223–252, 1998.

Tan, K. A., and S. D. Eckermann, Numerical simulation of mountain waves in the middle atmosphere over the southern Andes, in *Atmospheric Science Across theStratopause*, *Geophys. Monogr. Ser.*, vol. 123, edited by D. E. Siskind, S. D. Eckermann, and M. E. Summers, pp. 311–318, AGU, Washington, D. C., 2000.

Trenberth, K. E., and T. J. Hoar, The 1990–1995 El Niño-Southern Oscillation Event: Longest on record, *Geophys. Res. Lett.*, *23*, 57–59, 1996.

Tsuda, T., M. Nishida, C. Rocken, and R. H. Ware, A global morphology of gravity wave activity in the stratosphere revealed by the GPS occultation data (GPS/MET), *J. Geophys. Res.*, *105*, 7257–7273, 2000.

Wu, D. L., Horizontal wavenumber spectrum of MLS radiances, *J. Atmos. Sol. Terr. Phys.*, *63*, 1465–1477, 2001.

Wu, D. L., and J. W. Waters, Satellite observations of atmospheric variances: A possible indication of gravity waves, *Geophys. Res. Lett.*, *23*, 3631–3634, 1996a.

Wu, D. L., and J. W. Waters, Gravity-wave-scale temperature fluctuations seen by the UARS MLS, *Geophys. Res. Lett.*, *23*, 3289–3292, 1996b.

Wu, D. L., and J. W. Waters, Observations of gravity waves with the UARS Microwave Limb Sounder, in *Gravity Wave Processes*, *NATO ASI Ser., Ser. I*, vol. 50, pp. 103–120, Springer-Verlag, New York, 1997.

J. H. Jiang and D. L. Wu, Jet Propulsion Laboratory, California Institute of Technology, Mail Stop 183-701, 4800 Oak Grove Drive, Pasadena, CA 91109-8099, USA. (jonatha@mls.jpl.nasa.gov)

S. D. Eckermann, Middle Atmosphere Dynamics Section, Naval Research Laboratory, Washington D. C., USA.